2014

# Monodisperse MPt (M = Fe, Co, Ni, Cu, Zn) Nanoparticles Prepared from a Facile Oleylamine Reduction of Metal Salts

Yongsheng Yu
*Brown University, Harbin Institute of Technology*

Weiwei Yang
*Brown University, Harbin Institute of Technology*

Xiaolian Sun
*Brown University*

Wenlei Zhu
*Brown University*

Xingzhong Li
*University of Nebraska-Lincoln*, xli2@unl.edu

***See next page for additional authors***

Published in *Nano Letters* 14 (2014), pp. 2778−2782; doi: 10.1021/nl500776e

Submitted February 28, 2014; revised March 26, 2014; published April 1, 2014.

The authors declare no competing financial interest.

Supporting information for this article is available following the references.

# Monodisperse MPt (M = Fe, Co, Ni, Cu, Zn) Nanoparticles Prepared from a Facile Oleylamine Reduction of Metal Salts

Yongsheng Yu,[1,3] Weiwei Yang,[1,2] Xiaolian Sun,[1] Wenlei Zhu,[1] X.-Z. Li,[3]

D. J. Sellmyer,[3] and Shouheng Sun[1]

1. Department of Chemistry, Brown University, Providence, Rhode Island 02912, United States
2. School of Chemical Engineering and Technology, Harbin Institute of Technology, Harbin, Heilongjiang 150001, China
3. Nebraska Center for Materials and Nanoscience, University of Nebraska, Lincoln, Nebraska 68588, United States

*Corresponding author* – Shouheng Sun, email ssun@brown.edu

**Abstract**

We report a simple yet general approach to monodisperse MPt (M = Fe, Co, Ni, Cu, Zn) nanoparticles (NPs) by coreduction of $M(acac)_2$ and $Pt(acac)_2$ (acac = acetylacetonate) with oleylamine at 300°C. In the current reaction condition, oleylamine serves as the reducing agent, surfactant, and solvent. As an example, we describe in details the synthesis of 9.5 nm CoPt NPs with their compositions controlled from $Co_{37}Pt_{63}$ to $Co_{69}Pt_{31}$. These NPs show composition-dependent structural and magnetic properties. The unique oleylamine reduction process makes it possible to prepare MPt NPs with their physical properties and surface chemistry better rationalized for magnetic or catalytic applications.

**Keywords**: nanoparticles, oleylamine reduction, MPt alloy, alloy structure, nanomagnetism, catalysis

MPt nanoparticles (NPs) with M = Mn, Fe, Co, Ni, or Cu have attracted much attention in recent years due to their strong ferromagnetism (from FePt and CoPt)[1−6] and their much enhanced catalysis for electrochemical reactions.[6−15] These alloy NPs with controlled sizes and compositions are now routinely prepared either by decomposition/reduction of metal carbonyls and metal salts, or by coreduction of two metal salts. Despite the nearly precise control achieved on NP sizes and compositions, each of these previous syntheses is specific for one typical kind of MPt NPs. For example, thermal decomposition of $Fe(CO)_5$ and reduction of $Pt(acac)_2$ (acac = acetylacetonate) is commonly used to prepare monodisperse FePt NPs with Fe/Pt composition controls.[16−22] When this reaction is applied to prepare CoPt NPs via decomposition of $Co_2(CO)_8$ and reduction of $Pt(acac)_2$, only Pt-rich CoPt NPs can be produced.[23,24] The same is true for the synthesis of MnPt via decomposition of $Mn_2(CO)_{10}$ and reduction of $Pt(acac)_2$.[25,26] To prepare other types of MPt (M = Ni, Cu) NPs, metal salt coreduction has to be used because Ni and Cu carbonyls are not readily available.[27−29] In principle, metal salt reduction reaction should be a general approach to different MPt NPs, but the reduction potential differences between M- and Pt-salts and the need to control MPt nucleation and growth often require the use of a specific reducing agent for each synthesis.[30−32] Considering the sensitivity of MPt NP magnetism and catalysis over M/Pt compositions and surface chemistry, it is important to have a generalized synthetic process so that each kind of MPt NPs can be prepared in a very similar reaction condition and their magnetic and catalytic properties can be better controlled and compared.

Here, we report a facile, yet general, synthesis of monodisperse MPt (M = Fe, Co, Ni, Cu, Zn) alloy NPs via oleylamine (OAm) reduction of $M(acac)_2$ and $Pt(acac)_2$. OAm is widely used in the solution phase synthesis of NPs.[33] It is a primary amine with the boiling point around 350°C. Its −NH2 group has a relatively weak binding power to transition metals, especially to later transition metals. This, plus its long hydrocarbon chain, makes OAm an ideal surfactant to control NP growth, NP stabilization, and NP surface chemistry. Furthermore, OAm can also function as a weak reducing agent in high-temperature solution phase syntheses of metal and metal oxide NPs.[34−36] The unique feature of our synthesis is that OAm serves as the solvent, surfactant, and reducing agent and the desired MPt NPs are prepared simply by reacting $M(acac)_2$ and $Pt(acac)_2$ in OAm at 300°C. The size of the MPt NPs can be readily controlled and the M/Pt compositions are tuned by the molar ratios of $M(acac)_2/Pt(acac)_2$. Our synthesis simplifies the NP nucleation and growth condition, making it possible to rationalize the NP structural and surface properties for magnetic and catalytic applications.

As an example, we first demonstrated the synthesis of CoPt NPs. In a typical synthesis, 0.5 mmol of $Co(acac)_2$, 0.5 mmol of $Pt(acac)_2$, and 20 mL of OAm were first mixed at room temperature. Then the solution was heated to 300°C at a heating rate of 5°C/min and kept at 300°C for 1 h before it was cooled down to room temperature. The product was separated, purified, and redispersed in hexane. This synthesis gave $Co_{47}Pt_{53}$ as analyzed by inductively coupled plasma-atomic emission spectroscopy (ICP-AES).

The $Co_{47}Pt_{53}$ NP size and shape were analyzed by transmission electron microscopy (TEM) (fig. 1A). Most of the NPs are polyhedral, but a small fraction of them show an egg-like shape. The polyhedral NPs have an average diameter of 9.5 ± 0.8 nm. High-resolution TEM (HRTEM) image of a representative $Co_{47}Pt_{53}$ NP (fig. 1B) shows that the NP has the

well-defined and uniformly spaced lattice fringes with the fringe distance measured to be 0.22 nm, corresponding to the (111) interplanar spacing (0.221 nm) in the face centered cubic (fcc) CoPt alloy structure. X-ray diffraction (XRD) patterns of the NP assemblies (Supporting Information fig. S1) show the typical (111), (200), and (220) diffractions of the fcc-CoPt. The results from both HRTEM and XRD analyses indicate that CoPt NPs have a solid solution structure. The alloy structure is further characterized by the high-angle annular dark field (HAADF) image and by the atomically resolved scanning transmission electron microscopy-EDS (STEM-EDS) of four representative $Co_{47}Pt_{53}$ NPs (fig. 1C–H). The uniform distribution of Co (red) and Pt (green) within each NP is clearly seen (fig. 1D–G), which is also confirmed by linear scan EDS analysis across a $Co_{47}Pt_{53}$ NP (fig. 1H). These characterizations prove that in the current reaction condition, OAm can facilitate the nucleation and growth of CoPt into the solid solution structure.

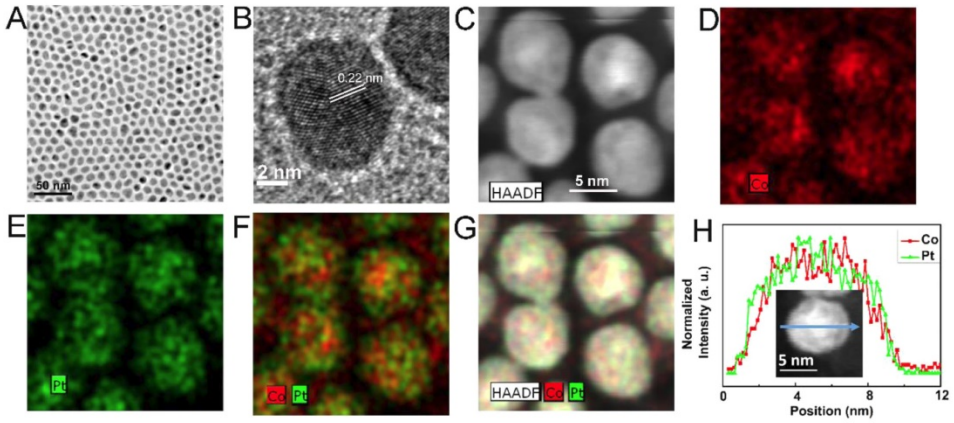


**Figure 1.** (A) TEM image of the 9.5 nm $Co_{47}Pt_{53}$ NPs. (B) HRTEM image of a representative NP shown in (A). (C) HAADF image of four representative $Co_{47}Pt_{53}$ NPs. (D–F) Elemental mappings of Co (red)/Pt (green) signals combined (F) and single element Co (red) (D) and Pt (green) (E). (G) HAADF image and the corresponding elemental map of four representative $Co_{47}Pt_{53}$ NPs. (H) EDS line scan crossing a $Co_{47}Pt_{53}$ NP. The inset shows the NP scanned.

The composition of the CoPt NPs could be tuned by the amounts of $Co(acac)_2$ added in the synthesis. We found that by keeping the amount of $Pt(acac)_2$ constant at 0.5 mmol and changing the amount of $Co(acac)_2$ from 0.3 to 1.0 mmol, Co contents in the NPs were controlled from 37 to 69%. The amount of $Co(acac)_2$ added in the synthesis and the final Co and Pt contents in NPs have a linear fitting (fig. 2A), indicating that it is easy to tune the compositions of the NPs by changing the amounts of two metal precursors. Figure 2B,C and Supporting Information figure S2 show the TEM images of the CoPt NPs of three compositions ($Co_{37}Pt_{63}$, $Co_{59}Pt_{41}$, and $Co_{69}Pt_{31}$). Despite the change in composition, these NPs have very similar size (9.5 nm) and size distribution. The XRD patterns of these CoPt NPs (Supporting Information fig. S1) show similar patterns that belong to the fcc-CoPt struc-

ture. With the Co composition in NPs increased, the (111) peaks shift to higher angle, indicating the reduction of (111) interplanar spacing. The relationship between the lattice constants *a* derived from the XRD patterns and the Co compositions in the NPs is shown in figure 2D. There is a typical linear relationship between the lattice constants a and the Co compositions (Vegard's law), confirming that all as-synthesized NPs have a solid solution structure.

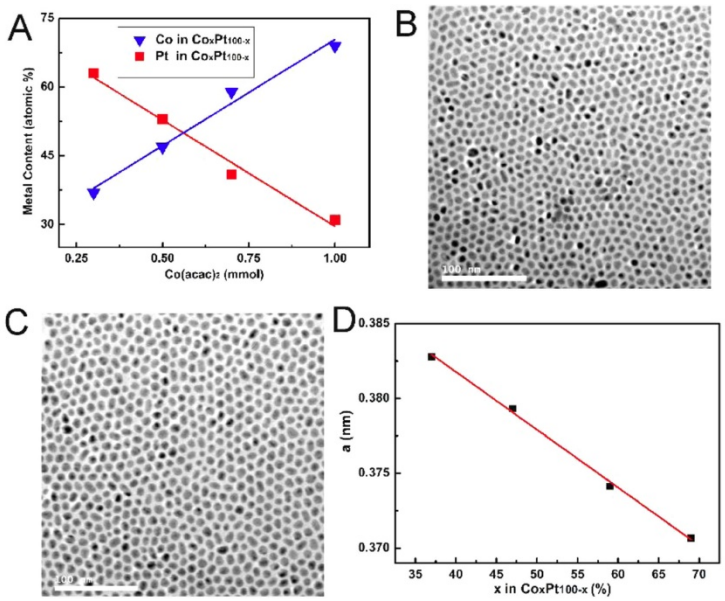


**Figure 2.** (A) Relationship between the amount of Co precursor and the Co and Pt contents within the NPs at constant $Pt(acac)_2$ of 0.5 mmol. TEM images of the 9.5 nm (B) $Co_{37}Pt_{63}$ and (C) $Co_{59}Pt_{41}$ NPs. (D) The relationship between the lattice constants *a* and the Co compositions in the NPs.

To have a better understanding on the CoPt NP growth in the current OAm reduction condition, we monitored NP formation at different reaction temperatures (130−300°C). At 130°C, no NPs were separated. NPs started to form after heating at 150°C for 1 h. However, the size and morphology of the NPs were not uniform, having a mixture of round and star-shaped NPs and nanorods (Supporting Information fig. S3A) and the NPs had an average composition of $Co_{40}Pt_{60}$. XRD patterns of these NPs showed the typical diffraction peaks of the fcc-CoPt (Supporting Information fig. S4). When the reaction temperature was raised to 200°C, the NPs have the polyhedral morphology (Supporting Information fig. S3B). The NP composition approached $Co_{47}Pt_{53}$, the final composition from the CoPt product separated from 300°C reaction. As a control, we reacted only $Pt(acac)_2$ or $Co(acac)_2$ with OAm at 150°C. We found that reaction of OAm with $Pt(acac)_2$ led to the formation of star-shaped fcc-Pt NPs as confirmed by TEM (Supporting Information fig. S3C) and XRD (Supporting Information fig. S4), while reaction with $Co(acac)_2$ yielded very small amount of Co NPs (Supporting Information fig. S3D). XRD patterns of these Co NPs (Supporting Information

fig. S4) contained peaks from hexagonal close-packed (hcp)-Co, $Co_3O_4$, and CoO in which the oxide peaks must originate from the oxidation of Co NPs. These results suggest that OAm can reduce both $Pt(acac)_2$ and $Co(acac)_2$ at 150°C, and the Co-reduction/nucleation/growth process was slower than the Pt-one. This series of experiments confirm that OAm can indeed reduce both $Pt(acac)_2$ and $Co(acac)_2$, and the formed Pt and Co atoms tend to nucleate together to form CoPt NPs with a solid solution structure.

In all the syntheses of CoPt we have described, $Pt(acac)_2$ was fixed to be 0.5 mmol. In this case, 9.5 nm CoPt NPs were separated and their sizes seemed to be independent of the Co/Pt composition changes. Alternatively, the sizes of the CoPt NPs could be controlled by adding borane *t*-butylamine (BBA), a slightly stronger reducing agent than OAm, to promote metal salt reduction and CoPt formation. For example, mixing 1.1, 0.55, and 0.275 mmol BBA in the reaction mixture containing 0.5 mmol of $Co(acac)_2$, 0.5 mmol of $Pt(acac)_2$, and 20 mL of OAm led to the formation of around 3.5 ± 0.4 nm $Co_{39}Pt_{61}$, 5.0 ± 0.5 nm $Co_{41}Pt_{59}$, and 7.5 ± 0.7 nm $Co_{45}Pt_{55}$ NPs, respectively (Supporting Information fig. S5A−C). In the synthesis, the color of the reaction solution changed from dark red to black at around 70, 75, and 80°C when 1.1, 0.55, and 0.275 mmol BBA were added in the reaction, respectively. As a comparison, without BBA, the color of the reaction solution turned to black at round 140°C. These indicate that the addition of BBA resulted in faster metal salt reduction and the formation of CoPt seeds, producing smaller NPs. XRD patterns of the as-synthesized NPs with different size show that all the NPs have fcc-CoPt structure (Supporting Information fig. S6).

The OAm-initiated reaction can be extended to the synthesis of other types of MPt NPs. Similar to what we have described in the study of CoPt NPs, we characterized these MPt NPs with TEM, XRD, and ICP-AES. For example, with the amount of $Pt(acac)_2$ fixed at 0.5 mmol in 20 mL OAm, adding 0.5 mmol each of $Zn(acac)_2$, $Cu(acac)_2$, $Fe(acac)_3$, and $Ni(acac)_2$ yielded 5.0 ± 0.5 nm $Zn_{48}Pt_{52}$, 6.0 ± 0.5 nm $Cu_{50}Pt_{50}$, 9.5 ± 1.0 nm $Fe_{49}Pt_{51}$, and 10 ± 1.5 nm $Ni_{46}Pt_{54}$ NPs with fcc-type solid solution structure (Supporting Information fig. S7 and S8). In the synthesis, we failed to produce MnPt with measurable Mn content in the attempted synthesis of MnPt with $Mn(acac)_2$ as the metal precursor. In such syntheses, a stronger reducing agent, such as BBA, should be added in the reaction mixture. From this series of syntheses, we can also see that OAm as a reducing agent is not strong enough to reduce $Mn(acac)_2$.

The OAm-controlled synthesis of MPt NPs makes it possible to study and compare MPt NP properties. As an example, we studied magnetic properties of the as-synthesized 9.5 nm CoPt NPs. All CoPt NPs are superparamagnetic at room temperature with their magnetic moment increasing with the Co content (fig. 3A). At 10 K, they are ferromagnetic (fig. 3B) with their saturated magnetizations ($M_s$) dependent on Co content in the NPs but their $H_c$ staying nearly constant at 1.0 kOe. This is consistent with what has been observed that magnetic moments of the alloy increase with the amount of ferromagnetic element present in the alloy structure and the coercivity is controlled by the magnetocrystalline anisotropy of the NPs. It further confirms that our CoPt NPs prepared from OAm reduction method have the same fcc-like solid solution structure.

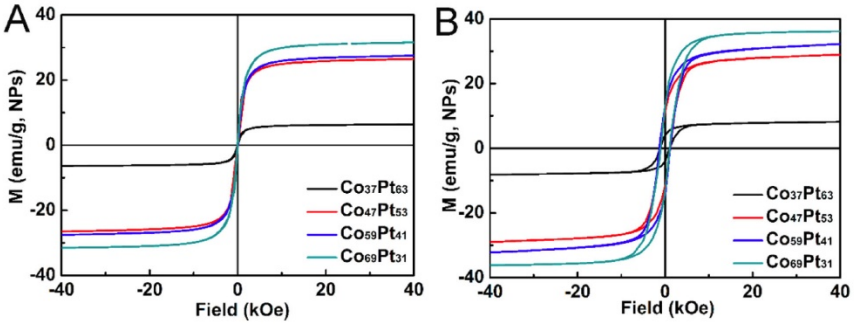


**Figure 3.** The hysteresis loops of the as-synthesized 9.5 nm CoPt NPs measured at (A) 300 K and (B) 10 K.

The changes of magnetization behavior of the CoPt NPs over temperature are studied by zero-field cooling (ZFC) and field cooling (FC) measurements.[37] Figure 4 shows the ZFC/FC curves of all four different kinds of CoPt NPs. From these ZFC/FC curves, we can see that all CoPt NPs are superparamagnetic at room temperature but their superparamagnetic blocking temperatures ($T_B$) increase from 105 to 205 K with increasing Co content from 37 to 69%. This indicates that increasing the ferromagnetic element Co content in the alloy structure might enhance the anisotropy barrier of the NPs, which could stabilize the magnetization transition within the CoPt alloy NPs.

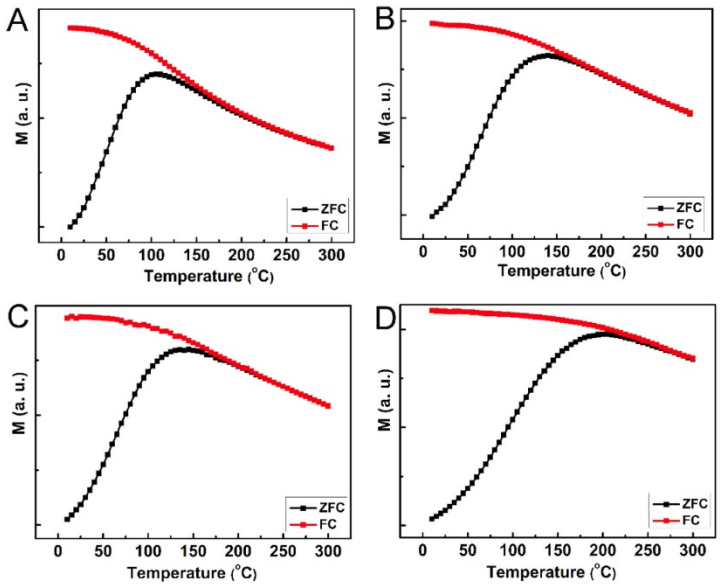


**Figure 4.** ZFC/FC curves of (A) $Co_{37}Pt_{63}$, (B) $Co_{47}Pt_{53}$, (C) $Co_{59}Pt_{41}$, and (D) $Co_{69}Pt_{31}$. The ZFC curves were obtained by cooling the sample in the absence of an external magnetic field and by measuring the *M* changes over temperature under a field of 100 Oe. The FC curves were obtained by cooling the sample under a magnetic field of 100 Oe and then measuring *M* changes over temperature.

When annealed, these fcc-structured NPs could be converted to an intermetallic face-centered tetragonal (fct) structure,[38] and fct-CoPt NPs showed strong ferromagnetism at room temperature. To achieve the structure transformation, we annealed the 9.5 nm CoPt NPs at 600 °C under Ar + 4% $H_2$ for 1 h. Figure 5A shows the room temperature hysteresis loop of the annealed $Co_{47}Pt_{53}$ NPs. They have room-temperature coercivity ($H_c$) at 4.3 kOe and $M_{max}$ at 28.7 emu/g (annealed sample). Other types CoPt NPs were also annealed, and they all showed ferromagnetic properties. Figure 5B summarizes the Co-composition dependent $M_{max}$ (at 15 kOe) and $H_c$ data for different CoPt NPs annealed at 600°C under Ar + 4% $H_2$ for 1 h. We can see that $M_{max}$ of the annealed samples increase linearly with the Co-component and $H_c$ show a maximum at 4.3 kOe. The $H_c$ change is consistent with what have been observed that CoPt alloys with Co/Pt near one can form better ordered fct structure and show stronger ferromagnetism.

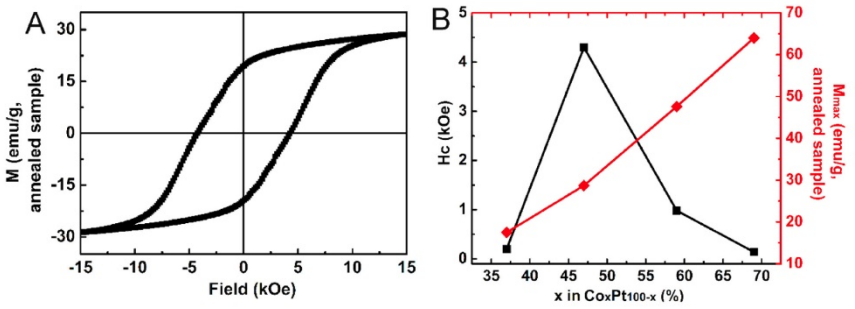


**Figure 5.** (A) Hysteresis loops of the annealed $Co_{47}Pt_{53}$ NPs and (B) Co-composition dependent $M_{max}$ (at 15 kOe) and $H_c$ for the annealed CoPt samples. The annealing was performed at 600°C under Ar + 4% $H_2$ for 1 h.

In summary, we have demonstrated a facile synthesis of monodisperse CoPt NPs by coreduction of $Co(acac)_2$ and $Pt(acac)_2$ with OAm at 300°C. The unique feature of this synthesis is that OAm in the synthesis serves as surfactant, solvent, and reducing agent. The NP size is controlled at 9.5 nm, and the compositions are tuned by the molar ratios of metal precursors. The synthetic controls achieved in both NP size and compositions in a very similar reaction condition allow detailed studies on their magnetic properties. All CoPt NPs are superparamagnetic at room temperature with their magnetic moments increasing linearly with the Co-composition in CoPt structure. Once annealed, the CoPt NPs can become room temperature ferromagnets with the $Co_{47}Pt_{53}$ NPs showing the highest $H_c$ of 4.3 kOe. The synthesis is not limited to CoPt NPs but can be extended to FePt, NiPt, CuPt, and ZnPt as well. It represents a general approach to Pt-based bimetallic NPs and will enable the detailed investigation of Pt-based alloy NPs for various magnetic or catalytic applications.

**Acknowledgments** – This work was supported by the U.S. Department of Energy, Office of Energy Efficiency and Renewable Energy (EERE), under its Vehicle Technologies Program, through the Ames Laboratory. The Ames Laboratory is operated by Iowa State University under contract DE-

AC02-07CH11358. The research at Nebraska was supported by U.S. DOE/EERE, ARO W911NF-09-2-0099, NCMN-NRI (NSF-DMR-0960110, D.J.S.) and Central Facilities of the Nebraska Center for Materials and Nanoscience, which is supported by the Nebraska Research Initiative.

## References

(1) Sun, S. H.; Murray, C. B.; Weller, D.; Folks, L.; Moser, A. *Science* 2000, 287, 1989−1992.

(2) Zeng, H.; Li, J.; Liu, J. P.; Wang, Z. L.; Sun, S. H. *Nature* 2002, 420, 395−398.

(3) Sun, S. H. *Adv. Mater.* 2006, 18, 393−403.

(4) Zeng, H.; Yan, M. L.; Powers, N.; Sellmyer, D. J. *Appl. Phys. Lett.* 2002, 80, 2350−2352.

(5) Tzitzios, V.; Niarchos, D.; Gjoka, M.; Boukos, N.; Petridis, D. *J. Am. Chem. Soc.* 2005, 127, 13756−13757.

(6) Poudyal, N.; Chaubey, G. S.; Rong, C.; Liu, J. P. *J. Appl. Phys.* 2009, 105, 07A749−07A751.

(7) Guo, S. J.; Zhang, S.; Sun, S. H. *Angew. Chem., Int. Ed.* 2013, 52, 8526−8544.

(8) Wang, C.; Chi, M.; Li, D.; van der Vliet, D.; Wang, G.; Lin, Q.; Mitchell, J. F.; More, K. L.; Markovic, N. M.; Stamenkovic, V. R. *ACS Catal.* 2011, 1, 1355−1359.

(9) Liu, Q.; Yan, Z.; Henderson, N. L.; Bauer, C. J.; Goodman, W.D.; Batteas, J. D.; Schaak, E. R. *J. Am. Chem. Soc.* 2009, 131, 5720−5721.

(10) Kang, Y.; Pyo, J. B.; Ye, X.; Gordon, T. R.; Murray, B. C. *ACS Nano* 2012, 6, 5642−5647.

(11) Kim, J.; Lee, Y.; Sun, S. H. *J. Am. Chem. Soc.* 2010, 132, 4996−4997.

(12) Wang, C.; Chi, M.; Li, D.; Strmcnik, D.; van der Vliet, D.; Wang, G.; Komanicky, V.; Chang, K.-C.; Paulikas, A. P.; Tripkovic, D.; Pearson, J.; More, L. K.; Markovic, M. N.; Stamenkovic, R. V. *J. Am. Chem. Soc.* 2011, 133, 14396−14403.

(13) Wang, C.; van der Vliet, D.; More, K. L.; Zaluzec, N. J.; Peng, S.; Sun, S.; Daimon, H.; Wang, G.; Greeley, J.; Pearson, J.; Paulikas, A. P.; Karapetrov, G.; Strmcnik, D.; Markovic, N. M.; Stamenkovic, V. R. *Nano Lett.* 2011, 11, 919−926.

(14) Zhang, J.; Fang, J. Y. *J. Am. Chem. Soc.* 2009, 131, 18543−18547.

(15) Guo, S. J.; Zhang, S.; Su, D.; Sun, S. H. *J. Am. Chem. Soc.* 2013, 135, 13879−13884.

(16) Sun, S. H.; Fullerton, E. E.; Weller, D.; Murray, C. B. *IEEE Trans. Magn.* 2001, 37, 1239−1243.

(17) Chen, M.; Liu, J. P.; Sun, S. H. *J. Am. Chem. Soc.* 2004, 126, 8394−8395.

(18) Zeng, H.; Li, J.; Wang, Z. L.; Liu, J. P.; Sun, S. H. *Nano Lett.* 2004, 4, 187−190.

(19) Chen, M.; Pica, T.; Jiang, Y. B.; Li, P.; Yano, K.; Liu, J. P.; Datye, A. K.; Fan, H. *J. Am. Chem. Soc.* 2007, 129, 6348−6349.

(20) Wang, C.; Hou, Y. L.; Kim, J.; Sun, S. H. *Angew. Chem., Int. Ed.* 2007, 46, 6333−6335.

(21) Kim, J.; Rong, C. B.; Lee, Y.; Liu, J. P.; Sun, S. H. *Chem. Mater.* 2008, 20, 7242−7245.

(22) Kim, J.; Rong, C. B.; Liu, J. P.; Sun, S. H. *Adv. Mater.* 2009, 21, 906−909.

(23) Shevchenko, V. E.; Talapin, V. D.; Rogach, L. A.; Kornowski, A.; Haase, M.; Weller, H. *J. Am. Chem. Soc.* 2002, 124, 11480−11485.

(24) Pellegrino, T.; Fiore, A.; Carlino, E.; Giannini, C.; Cozzoli, D. P.; Ciccarella, G.; Respaud, M.; Palmirotta, L.; Cingolani, R.; Manna, L. *J. Am. Chem. Soc.* 2006, 128, 6690−6698.

(25) Lee, D. C.; Ghezelbash, A.; Stowell, C. A.; Korgel, B. A. *J. Phys. Chem. B* 2006, 110, 20906−20911.

(26) Kang, Y. J.; Murray, C. B. *J. Am. Chem. Soc.* 2010, 132, 7568−7569.

(27) Ahrenstorf, K.; Albrecht, O.; Heller, H.; Kornowski, A.; Golitz, D.; Weller, H. *Small* 2007, 3, 271−274.

(28) Ahrenstorf, K.; Heller, H.; Kornowski, A.; Broekaert, J. A. C.; Weller, H. *Adv. Funct. Mater.* 2008, 18, 3850−3856.

(29) Zhu, H. Y.; Zhang, S.; Guo, S. J.; Su, D.; Sun, S. H. *J. Am. Chem. Soc.* 2013, 135, 7130−7133.

(30) Chen, M.; Nikles, E. D. *Nano Lett.* 2002, 2, 211−214.

(31) Wang, H.; Shang, P.; Zhang, J.; Guo, M.; Mu, Y.; Li, Q.; Wang, H. *Chem. Mater.* 2013, 25, 2450−2454.

(32) Reiss, B. D.; Mao, C.; Solis, D. J.; Ryan, K. S.; Thomson, T.; Belcher, A. M. *Nano Lett.* 2004, 4, 1127−1132.

(33) Mourdikoudis, S.; Liz-Marzán, M. L. *Chem. Mater.* 2013, 25, 1465−1476.

(34) Nam, K. M.; Shim, J. H.; Ki, H.; Choi, S. I.; Lee, G.; Jang, J. K.; Jo, Y.; Jung, M. H.; Song, H.; Park, J. T. *Angew. Chem., Int. Ed.* 2008, 47, 9504−9508.

(35) Chaubey, G. S.; Barcena, C.; Poudyal, N.; Rong, C.; Gao, J.; Sun, S.; Liu, J. P. *J. Am. Chem. Soc.* 2007, 129, 7214−7215.

(36) Hou, Y.; Xu, Z.; Sun, S. *Angew. Chem., Int. Ed.* 2007, 46, 6329−6332.

(37) Bigot, J.-Y.; Kesserwan, H.; Halté, V.; Ersen, O.; Moldovan, M. S.; Kim, T. H.; Jang, J.; Cheon, J. *Nano Lett.* 2012, 12, 1189−1197.

(38) Sun, C.; Jia, Z. Y.; Huang, Y. H.; Harrell1, J. W.; Nikles, D. E.; Sun, K.; Wang, L. M. *J. Appl. Phys.* 2004, 95, 6747−6749.

**Supporting Information**

***Materials and Methods***

*Materials*

Oleylamine (OAm, >70%), $Pt(acac)_2$ (acac=aceylacetonate) (99%), Cobalt(II) acetylacetonate ($Co(acac)_2$) hydrate (97%), Zinc(II) acetylacetonate ($Zn(acac)_2$) hydrate, Copper(II) acetylacetonate ($Cu(acac)_2$) (97%), Iron(III) acetylacetonate ($Fe(acac)_3$) (99%), Nickel(II) acetylacetonate ($Ni(acac)_2$) (95%), Borane *t*-butylamine (BBA) (97%), hexane (98.5%), isopropanol (99.5%), ethanol (100%) were all purchased from Sigma Aldrich.

*Characterization*

X-ray diffraction (XRD) characterization was carried out on a Bruker AXS D8-Advanced diffractometer with Cu $K\alpha$ radiation ($\lambda$ = 1.5418 Å). The inductively coupled plasma-atomic emission spectroscopy (ICP-AES) analyses were carried on a JY2000 Ultrace ICP Atomic Emission Spectrometer equipped with a JY AS 421 autosampler and 2400g/mm holographic grating. Samples for transmission electron microscopy (TEM) analysis were prepared by depositing a single drop of diluted particle dispersion in hexane on amorphous carbon coated copper grids. TEM images were obtained with a Philips CM 20 operating at 200 kV. High-resolution TEM (HRTEM) and the atomically resolved scanning transmission electron microscopy-EELS (STEM-EDS) images were obtained on a Fei Tecnai Osiris with an accerating votalage of 200 kV. Magnetic properties were measured by a Physical Properties Measurement System (PPMS) up to 70 kOe and a Lakeshore 7404 high sensitivity vibrating sample magnetometer (VSM) with fields up to 15 kOe.

*Synthesis of $Co_{47}Pt_{53}$ nanoparticles (NPs)*

0.5 mmol of $Co(acac)_2$, 0.5 mmol of $Pt(acac)_2$, and 20 mL of OAm were first mixed at room temperature. Then the solution was further heated to 300°C at a heating rate of 5°C/min and kept at 300°C for 1 h before it was cooled to room temperature. Then the heating source was removed, and the solution was cooled to room temperature, after which the solution was exposed to air. A black product was precipitated by adding 40 ml of ethanol, and separated by centrifugation. Finally, the product was dispersed in hexane.

*Synthesis of Zn48Pt52, Cu50Pt50, Fe49Pt51 and Ni46Pt54 NPs*

Under the conditions described in the synthesis of $Co_{47}Pt_{53}$ NPs, 0.5 mmol of $Pt(acac)_2$ and 20 mL of OAm were first mixed with 0.5 mmol $Zn(acac)_2$, 0.5 mmol $Cu(acac)_2$, 0.5 mmol $Fe(acac)_3$ and 0.5 mmol $Ni(acac)_2$ at room temperature, respectively. Then the solution was further heated to 300°C at a heating rate of 5°C/min and kept at 300°C for 1 h. Then the NPs were also separated and purified by using hexane, ethanol, and centrifugation. Finally, the particles were kept in hexane.

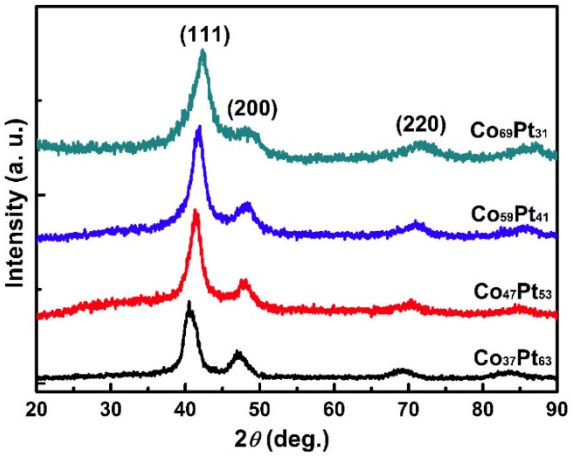


**Figure S1.** XRD patterns of CoPt NPs with different Co/Pt ratios.

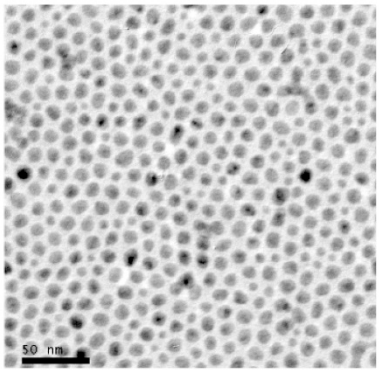


**Figure S2.** TEM image of the 9.5 nm $Co_{69}Pt_{31}$ NPs.

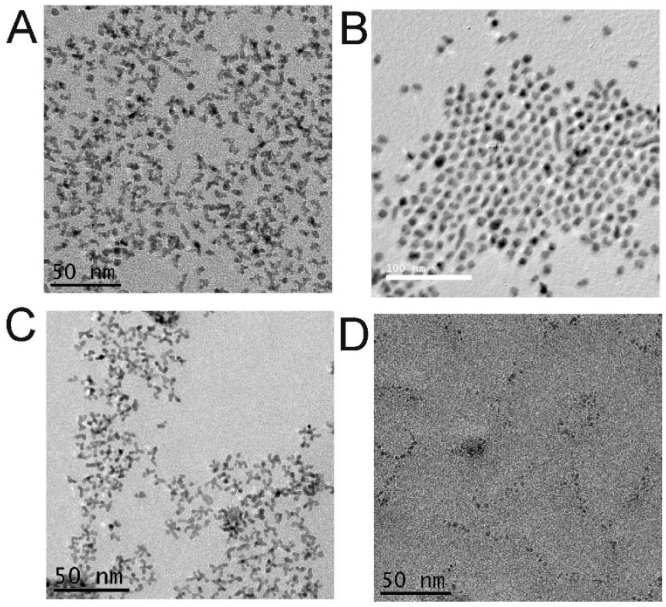


**Figure S3.** (A) $Co_{40}Pt_{60}$ synthesized at 150°C, (B) $Co_{47}Pt_{53}$ synthesized at 200°C, (C) Pt and (D) the mixture of Co, $Co_3O_4$, and CoO NPs synthesized at 150°C.

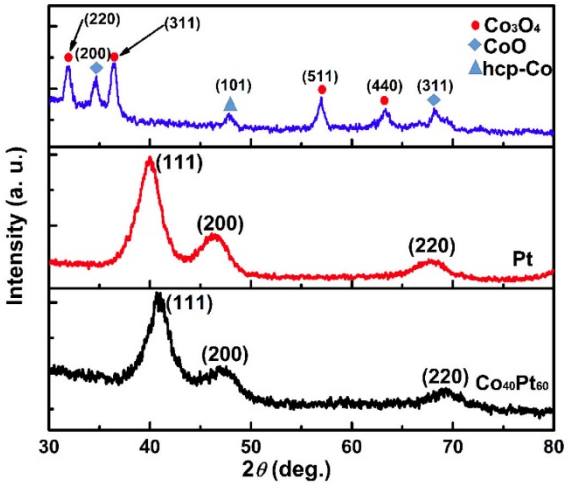


**Figure S4.** XRD patterns of $Co_{40}Pt_{60}$, Pt, and the mixture of Co, $Co_3O_4$, and CoO NPs synthesized at 150°C.

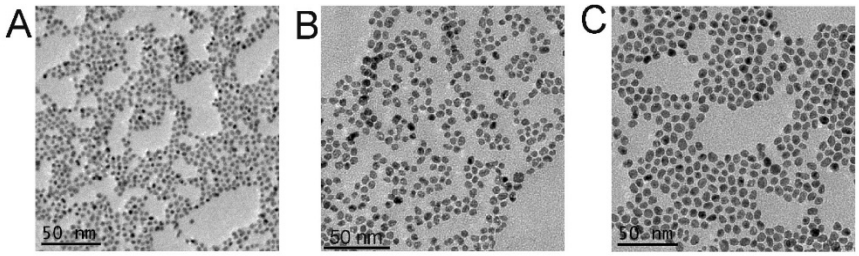


**Figure S5.** TEM images of (A) 3.5 nm $Co_{39}Pt_{61}$, (B) 5.0 nm $Co_{41}Pt_{59}$, and (C) 7.5 nm $Co_{45}Pt_{55}$ NPs synthesized by mixing 1.1, 0.55, and 0.275 mmol BBA with 20 mL OAm, respectively.

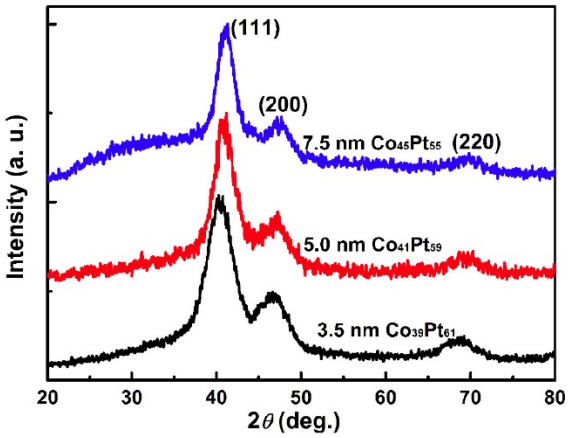


**Figure S6.** XRD patterns of 3.5 nm $Co_{39}Pt_{61}$, 5.0 nm $Co_{41}Pt_{59}$, and 7.5 nm $Co_{45}Pt_{55}$ NPs.

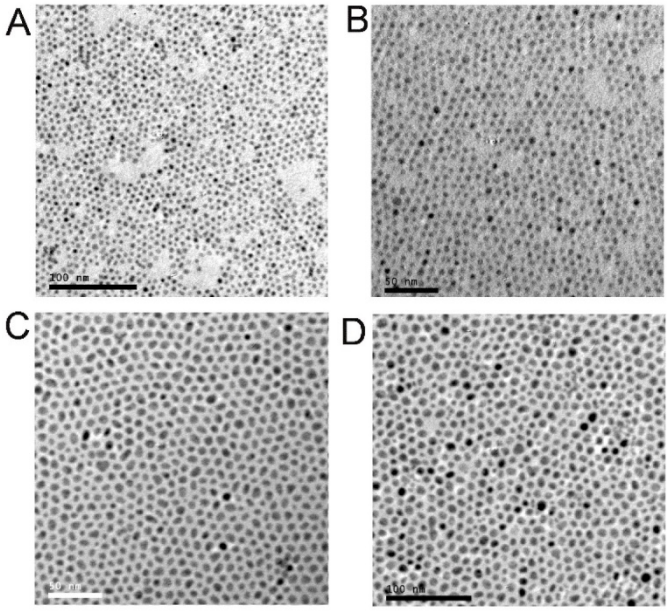


**Figure S7.** TEM images of (A) 5.0 nm $Zn_{48}Pt_{52}$, (B) 6.0 nm $Cu_{50}Pt_{50}$, (C) 9.5 nm $Fe_{49}Pt_{51}$, and (D) 10 nm $Ni_{46}Pt_{54}$ NPs.

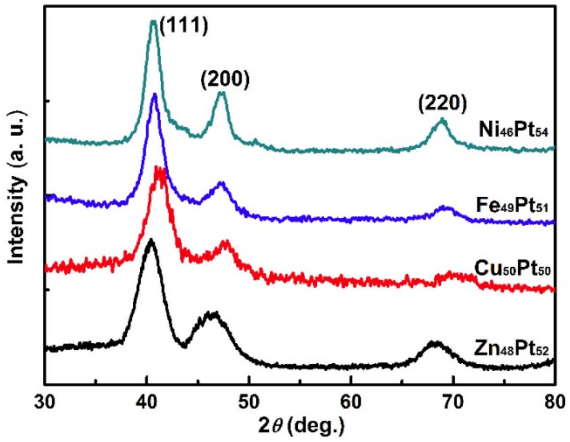


**Figure S8.** XRD patterns of $Zn_{48}Pt_{52}$, $Cu_{50}Pt_{50}$, $Fe_{49}Pt_{51}$, and $Ni_{46}Pt_{54}$ NPs.